Ligand Structure and Adsorption Free Energy of Nanocrystals on Solid Substrates

Matthew Pham[1] and Alex Travesset[2, a)]
[1)] *Department of Physics and Astronomy, Iowa State University, Ames, Iowa, 50011, United States*
[2)] *Department of Physics and Astronomy, Ames Laboratory and Iowa State University, Ames, Iowa, 50011, United States*

(Dated: 7 December 2020)

We present an investigation of alkylthiolated nanocrystals adsorbing to a solid substrate. We calculate adsorption free energies and report a number of effects induced by the substrate. Nearest neighbor distances and bonding free energies are significantly different than for a free floating case, there is a weakening of bonding free energies among nanocrystals, and adsorption is manifestly anisotropic, i.e., stronger along certain directions of the NC core. We contend that this last result accounts for the Bain transition (FCC $\rightarrow$ BCC) observed in experimental results. We report the presence of vortices induced by the substrate, which explain the increased nearest neighbor distance among nanocrystals, in excellent quantitative agreement with experimental results and with the predictions of the Orbifold Topological Model (OTM). Implications for the assembly of nanostructures and future experiments are also discussed.

I. INTRODUCTION

Nanocrystal (NC) materials hold the promise of solving many of the technological challenges of our times. At a fundamental level, it enables the possibility of programming matter to a degree that is not attainable with traditional atoms or molecules; there is virtually an infinite number of NCs, as the core maybe tuned according to composition, shape or size and the capping ligand by many other physical or chemical parameters[1,2].

The most common strategy for the assembly of bulk structures is solvent evaporation on a solid substrate[3–6]. A relevant question is, then, to what extent the substrate determines the nucleation and stability of the resulting three dimensional structure. This raises broader questions related to the adsorption of NCs on solid surfaces, as different experimental techniques such as solvent evaporation[7–11], Langmuir transfer from an assembly at air water interface[12,13] or capillarity forces[14] have been used to make NC materials on silicon, teflon, carbon, polyethylene oxide or silica substrates, among many others[15].

In previous papers, we have theoretically determined, by the Orbifold Topological Model (OTM)[17,18] and numerical simulations[19–23], the structure of both alkylthiolated and polystyrene[24] based NC assemblies. In all cases, both for bulk and two dimensional assemblies, we have not considered the effect of the solid substrate. This is particularly relevant in two dimensional systems, as it is not generally possible to experimentally assemble such systems without an interface. In this paper, we will be concerned with interfaces consisting of a solid substrate. Other interfaces, such as liquid-vapor or liquid-liquid interfaces, have been extensively discussed elsewhere and will not be studied here.

[a)] Electronic mail: trvsst@ameslab.gov

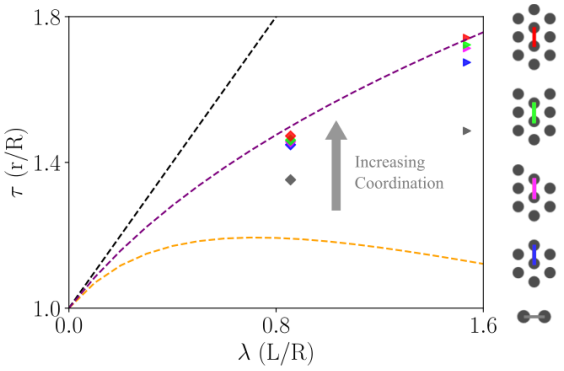

FIG. 1: NC separation, τ, as a function of ligand length, λ, as reported in the experiments of Boles and Talapin[16]. NC separation increases with coordination. Parameters τ and λ are defined in Eq. 2 and Eq. 1.

There are a number of interesting effects associated with two dimensional assemblies. In Ref.[16], Boles and Talapin thoroughly analyzed NC nearest neighbor distances as a function of coordination number, showing that they increases with coordination number, see Fig. 1. This is the expected behaviour within the OTM, where the separation of low coordinated NCs is determined by "vortices", i.e., splayed ligand conformations. There is excellent agreement of OTM predictions with experimental results[16,25] and with numerical simulations[19,21,22]. All these results, however, have been obtained for free floating systems. A substrate should be expected to play a relevant role, as it maybe regarded as a ligand free "giant" NC, and therefore it should be expected to alter ligand conformations by inducing vortices on the adsorbed NC, as we show further below, see Fig. 14 and specially Fig. 10. Furthermore, because there are only ligands between the core and the substrate, their interactions are expected to be more sensitive to the facets of

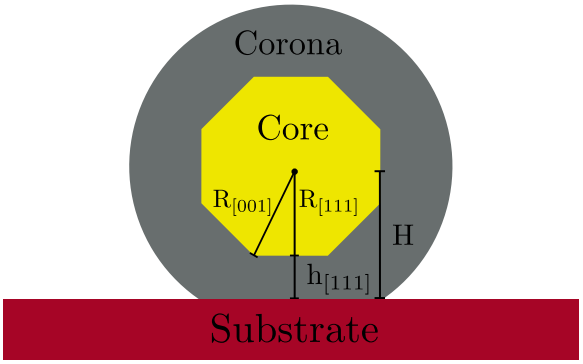

(a)

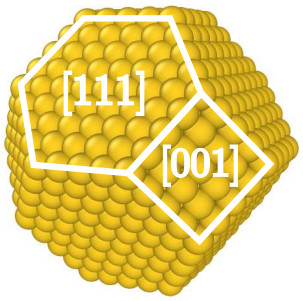

(b)

	(Å)		
NC	$R_{[001]}$	$R_{[111]}$	R
Au_{201}	7.92	6.86	10.15
Au_{1289}	15.84	13.72	18.23

(c)

FIG. 2: (a) Schematic showing variable naming convention of H (NC center to substrate), $R_{[ijk]}$ (NC core radius along direction), and $h_{[ijk]}$, ligand thickness at the substrate; (b) Image of Au core indicating [001] and [111] face; (c) Table with values $R_{[001]}$, $R_{[111]}$, and R for gold cores consisting of 201 and 1289 gold atoms.

the NC core, see Fig. 2. This may play a significant role in the reported metastable FCC phases nucleating near a solid substrate[26,27] before transforming into the BCC presumed equilibrium structure (Bain transition). Quantitative predictions for these effects is one of the goals for this paper.

The relevance of NC adsorption to solid substrates extends to many other relevant applications such as catalysis, heat conduction at the nanoscale, tribology, etc.[15]. There have been several numerical simulations addressing these applications[28–31] by methods closely related to the ones in this paper, and also by ab-initio studies, see Ref.[32]. Furthermore, although our investigation will be restricted to alkylthiolated NCs, the OTM has been successfully applied to other systems, such as dithiol linkers[33], interpolymer complexation[34], PEG based assembly[35] and Polystyrene NCs[24], thus making a clear case on the general interest of this study.

The organization of the paper is as follows: we first provide a description of the system to be investigated and the specifics of the substrates, followed by calculations of free energies, minimum NC separations and ligand conformations. A discussion of the implications follows together with the general conclusions and future prospects for these studies.

II. RESULTS

A. Model

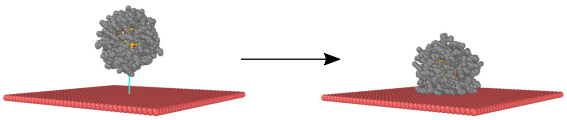

FIG. 3: Starting and end configuration for the calculation of the potential of mean force between the NC and the solid substrate, results in Fig. 8, for the $Au_{201}(SC_{12})_{80}$ system. The cyan link represents a harmonic bond.

NCs were modeled using the same force field as in previous studies, see Ref.[20] or the supplementary material for force field parameters. The NCs are truncated octahedron (TO) gold cores, see Fig. 2, grafted with saturated hydrocarbon chains. The NC core radius, R, is defined as the radius of a sphere with equal surface area to the core plus the bond length between the gold and sulfur atoms, as it has been discussed previously[19,22]. Gold cores consist of either 201 or 1289 atoms, as first considered in Ref.[36], and the ligands are hydrocarbon chains consisting of 9, 12, or 18 carbons. Following previous notations, NC cores will be referred as $Au_n(SC_mH_{2m+1})_j$, where n

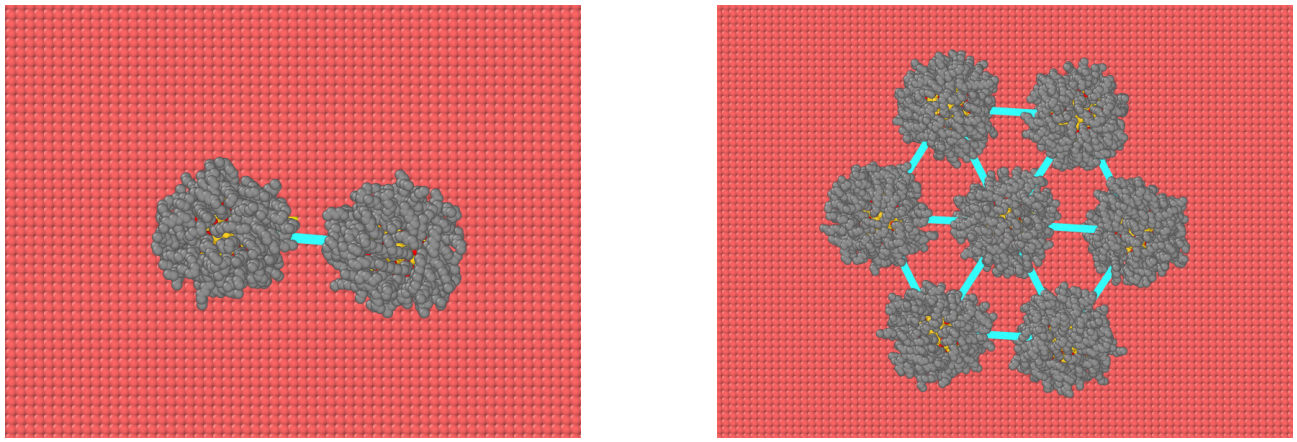

(a) (b)

FIG. 4: (a) Example snapshot of pair configuration. (b) Example snapshot of (6-3)S configuration. The cyan links represent harmonic bonds.

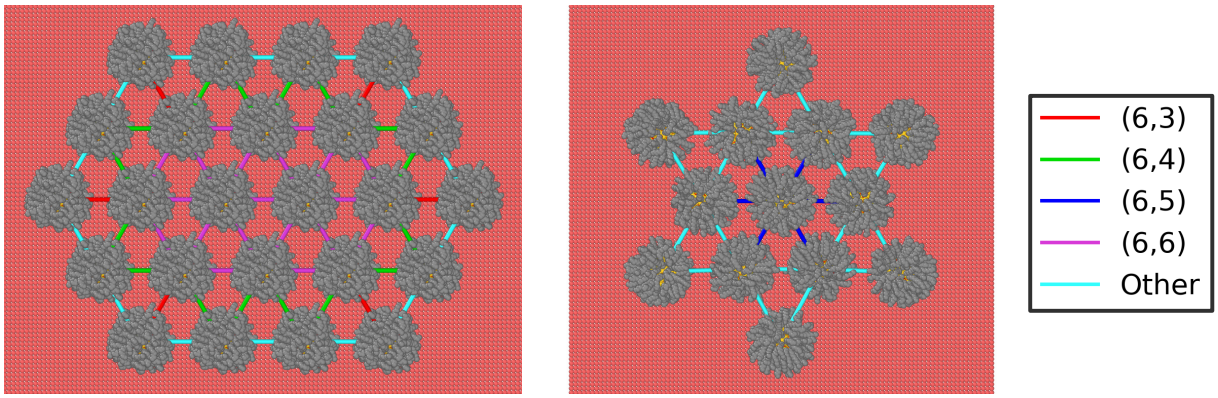

FIG. 5: Snapshots of initial NC cluster configurations labeled with bonds between NCs of different coordinations of interest.

is the number of gold atoms in the core, m is the number of carbons within each hydrocarbon chain, and j is the number of ligand chains grafted to the core.

The substrate was modeled as a rigid, single layer of gold atoms organized into a square grid with a lattice constant of 2.885 Å, which corresponds to the [001] gold surface. Other substrates maybe considered, but do not change any of the qualitative conclusions. Because there is strong attraction between ligands and substrates, we do not expect significant quantitative changes for other solid substrates. The overall dimensions of the substrate were large enough such that the NCs are insensitive to the Lennard-Jones potential cutoff and periodic boundary conditions. In all simulations, the substrate was kept fixed. The simulations were run using the HOOMD-blue package[37] with rigid body dynamics[38] and HOODLT for sample preparation and force field[39].

All simulations were run at $T = T_m = 387$, following our previous studies. A typical run consisted of $(1-5)\times 10^6$ time steps to equilibrate the systems and $(5-10)\times 10^6$ time steps for production runs. The general strategy for running simulations was to use harmonic bonds, or springs, to hold configurations in place to sample data and iteratively adjusting the bonds to sample different configurations. More details on the methodology and constraints of each simulation are described in sections below.

B. Single NC Adsorption to a Substrate

The Potential of Mean Force (PMF) for the NC and the solid substrate is calculated using the Weighted Histogram Analysis Method (WHAM)[40] in conjunction with umbrella sampling as previously done in our previous papers[20]. The NC was bonded to the substrate using harmonic bonds as represented in Fig. 3 by a cyan line. By preventing rotations of the core, the NC was transported towards the substrate keeping fixed orientations, see Fig. 2. We considered two different NC core sizes,

three different ligand lengths, and two orientations corresponding to the [100] and [111] directions, resulting in the 12 PMFs shown in Fig. 8 and summarized in Table I. Snapshots of NCs of all three core sizes and ligand lengths adsorbed onto the substrate are shown in the supplemental information.

	[001]		[111]	
NC-Substrate	F_{min} (k_BT)	H (Å)	F_{min} (k_BT)	H (Å)
$Au_{201}(SC_9)_{80}$	50	17.6	61	16.3
$Au_{201}(SC_{12})_{80}$	73	17.7	83	17.1
$Au_{201}(SC_{18})_{80}$	124	17.9	125	17.5
$Au_{1289}(SC_9)_{258}$	71	26.7	79	26.4
$Au_{1289}(SC_{12})_{258}$	116	26.8	123	26.4
$Au_{1289}(SC_{18})_{258}$	194	27.9	214	26.8
Symmetric NC Pair	$F_{min}/2$ (k_BT)		$\rho/2$ (Å)	
$Au_{201}(SC_9)_{80}$	36		13.85	
$Au_{201}(SC_{12})_{80}$	57		13.55	
$Au_{201}(SC_{19})_{80}$	103		13.8	
$Au_{1289}(SC_9)_{258}$	44		24.5	
$Au_{1289}(SC_{12})_{258}$	73		24.75	
$Au_{1289}(SC_{19})_{258}$	144		25.2	

TABLE I: Free energy minimum and separation distance, H, of NC-Substrate and symmetric NC-NC interactions. The "Symmetric NC pair" corresponds to the nearest neighbor distance, ρ, of an identical, free floating NC pair, i.e., no solid substrate. See Fig. 2 for notation.

The adsorption free energy is given by the minimum of the PMF in Fig. 8 and is listed in Table I with the equilibrium separation. The equilibrium separation is sensitive to the orientation $[ijk]$, as defined by Fig. 2, and is denoted by H in Table I.

C. Adsorption of many NCs to a Substrate

We consider many NCs adsorbed onto the solid substrate. Here, differently from the previous calculations, translation and rotation of the NCs were not constrained. The NC configurations were simply allowed to be adsorbed onto the substrate and relaxed for a sufficient amount of time prior to data collection. The calculations considers NCs with coordinations ranging from 1 to 6, as shown in Fig. 4. We analyze them in turn.

1. Pair Configuration (Coordination $n = 1$)

Two NCs were placed on the substrate sufficiently far away from each other, as shown in Fig. 4, and equilibrated. No bias potentials were necessary to hold the NCs onto the substrate as they are naturally held in place by the strong adsorption energies calculated above, see Table I. Umbrella sampling was performed by placing a harmonic bond between the two NCs and slowly reducing the spring equilibrium distance. The PMF is shown in Fig. 9. Compared with the same calculation in the absence of substrate, the PMF is virtually identical, except at sufficiently short distances, where the minimum is less deep and occurs at a larger separation.

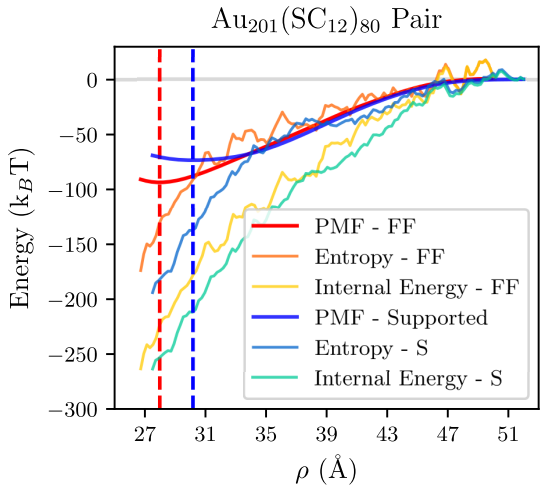

FIG. 9: Comparison of the $Au_{201}(SC_{12})_{80}$ pair configurations without a substrate (Free Floating) and with a substrate (Supported). Center-center separation of the PMF minimum in the presence of a substrate is increased by 2.19 Å relative to the free floating case. Separation between NC centers, ρ, is given in Å and free energy is given in k_BT with $T = T_M = 387$ K.

2. Coordinations $n = 3, 4, 5, 6$

Using the convention (M,N)S or (M,N)FF denoting the bond between a NC with M nearest neighbors and N nearest neighbors either supported by a substrate (S) or Free Floating (FF). We considered (6,6)S, (6,5)S, (6,4)S, and (6,3)S configurations. The cases (6,3)FF, (6,6)FF, Icos, and FCC configurations were obtained from previous studies[19–22].

Simulations of (6,3)FF and (6,3)S systems were run for $Au_{201}(SC_{12})_{80}$ and $Au_{1289}(SC_{12})_{258}$ NCs similar to the pair configuration. Simulations were conducted and run according to the methods described in Ref.[21]. NCs were held in place with harmonic bonds centered around a specific ρ for data collection and iteratively shortened to sample along various values of ρ. Results are shown in Fig. 6 and snapshots of average NC clusters and single NCs in the clusters are provided by the supplemental information.

In order to compare the nearest neighbor separations between NCs of higher coordinations, large NC clusters were simulated as shown in Fig. 5. NCs were initialized such that they are close enough to experience attraction,

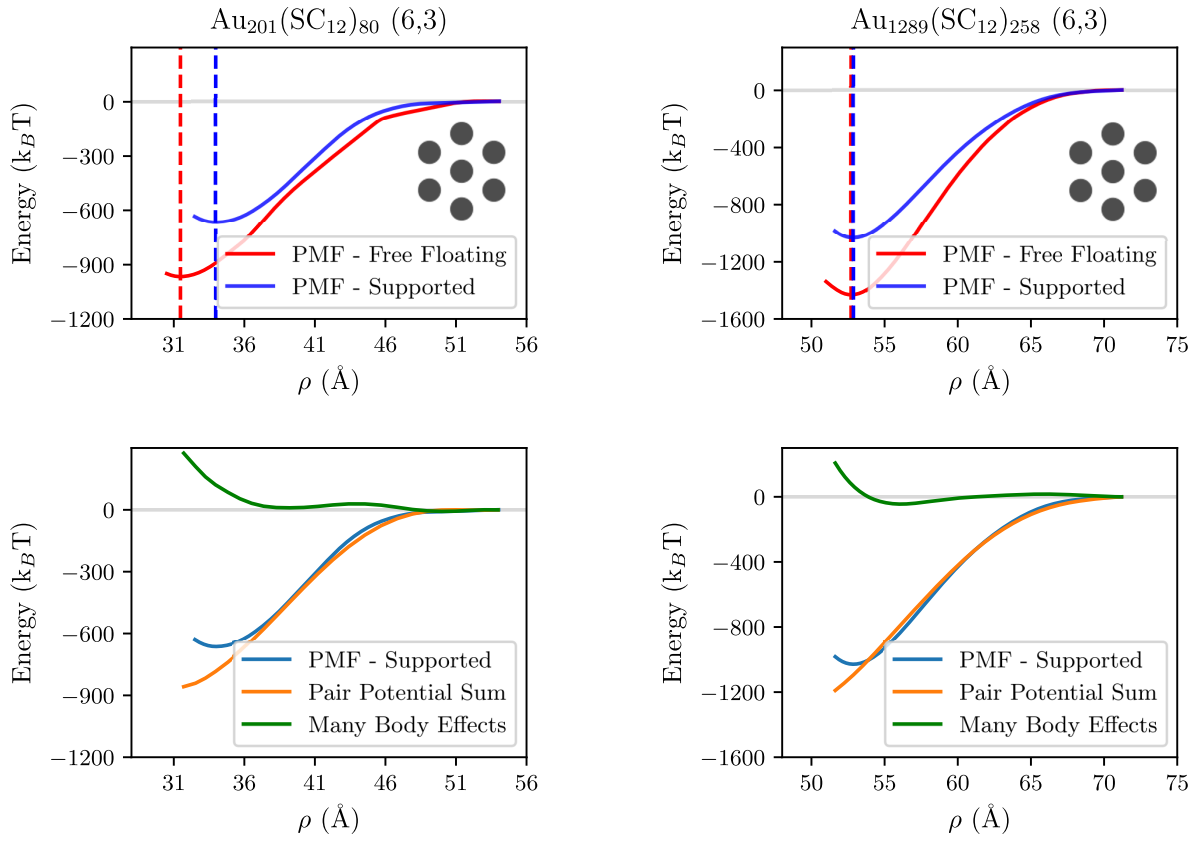

FIG. 6: Comparison of PMF for $Au_{201}(SC_{12})_{80}$ and $Au_{1289}(SC_{12})_{258}$ (6,3) systems. For $Au_{201}(SC_{12})_{80}$ (6,3), there is a 2.77 Å difference between the free floating and supported cases, while for $Au_{1289}(SC_{12})_{258}$ (6,3), there is only a 0.16 Å difference. (6,3)S and sum of (1,1)S pair potentials are also compared for both NC sizes. Separation between the center NC and the cage NCs, ρ, is given in Å and free energy is given in k_BT with $T = T_M = 387$ K.

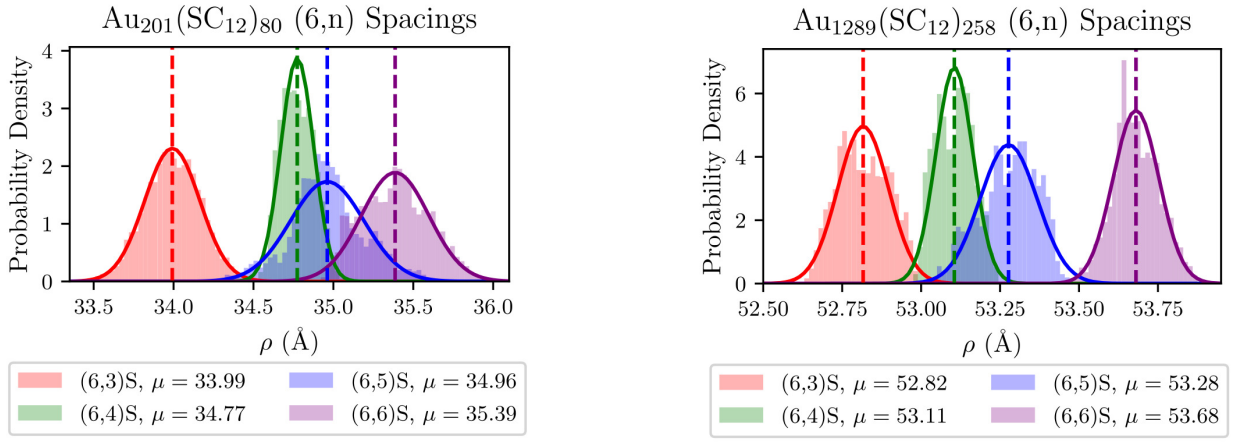

FIG. 7: Histograms of interparticle spacings of various (6,N) bonds in large, supported NC clusters.

but far from the expected equilibrium separation. Using an iterative equilibrating process, the outer most layer of NCs were allowed to move while the remaining NCs were held in place. After sufficient relaxation, the next layer of NCs was unfrozen and allowed to equilibrate such that two layers were unconstrained simultaneously. This process was repeated until all layers were unconstrained and given a sufficient amount of time to reach an equilib-

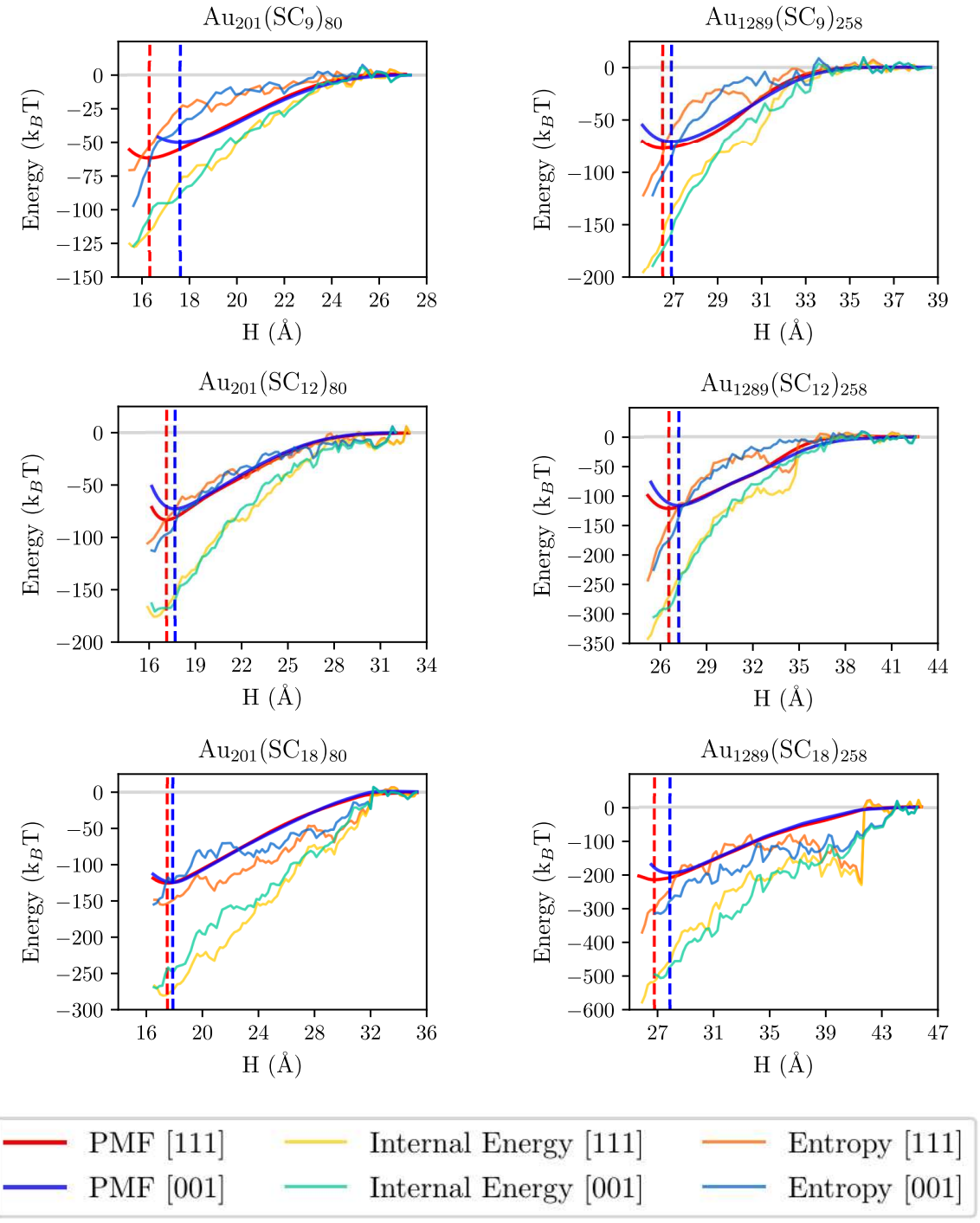

FIG. 8: Potential of mean force between NC and substrate for combinations of two core sizes, three hydrocarbon ligand lengths, and two orientations. Separation between NC center and substrate, H, is given in Å, and the free energy is given in k_BT, with $T = T_M = 387$ K. Dashed vertical lines indicate minimum of free energy.

rium separation. At this point, data collection began by simulating a completely unconstrained cluster and sampling the nearest neighbor separations between NCs of different coordinations, see Fig. 7.

III. DISCUSSION

We now discuss more extensively the numerical results by focusing on the NC nearest neighbor separation, the magnitude of the bonding energy and the different ligand

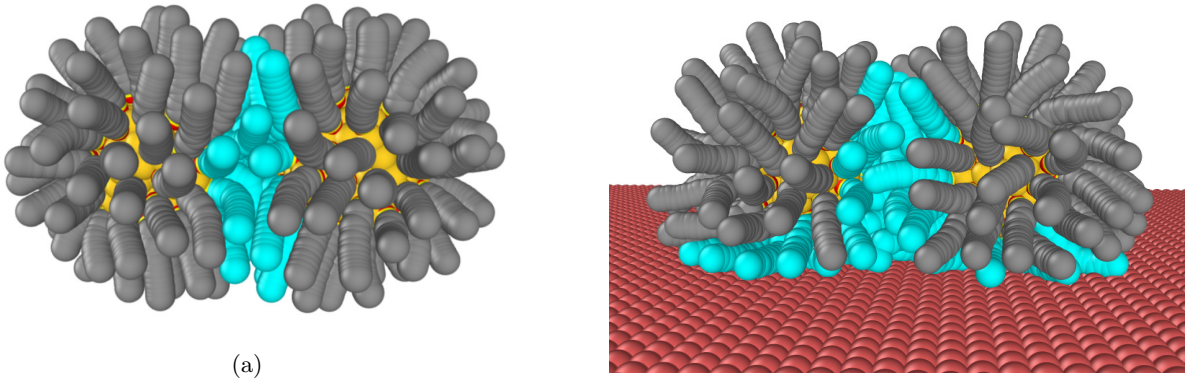

(a) (b)

FIG. 10: Average configuration of $Au_{201}(SC_{12})_{80}$ pairs in the free floating case (a) and on a solid substrate (b). The two vortices (on each NC) have different orientations. Ligands that are part of vortices are colored cyan.

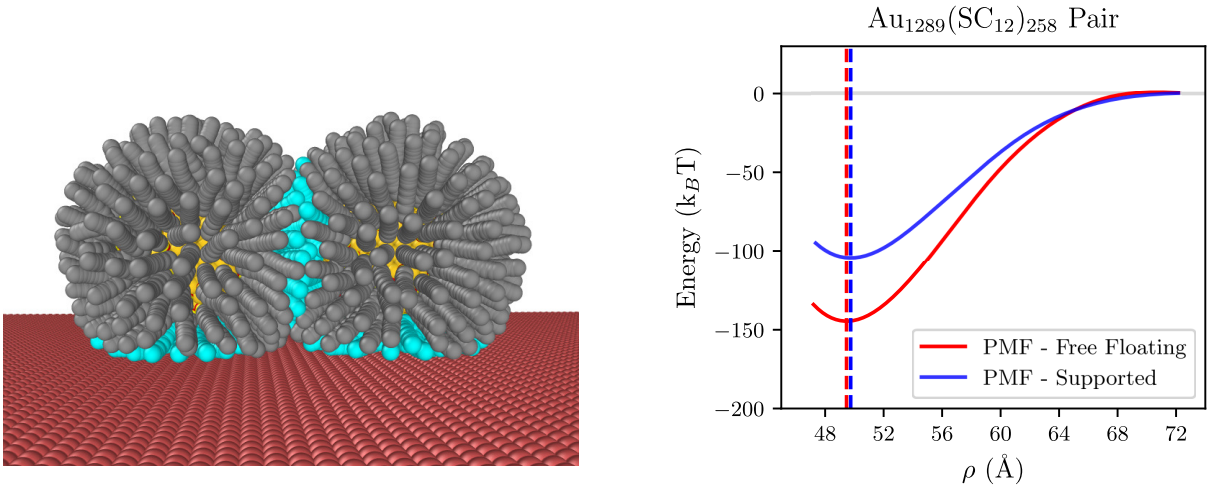

FIG. 11: Average configuration of $Au_{1289}(SC_{12})_{258}$ pair supported by a substrate with ligands part of vortices colored cyan (left). PMF comparison of $Au_{1289}(SC_{12})_{258}$ supported and free floating pairs (right). Center-center separation of the PMF minimum in the presence of a substrate is increased by 0.28 Å relative to free floating case. Separation between NC centers, ρ, is given in Å and free energy is given in k_BT with $T = T_M = 387$K

conformations. The relevant parameters characterizing the NCs and their nearest neighbor interactions are λ, τ, ξ, which are defined as

$$\lambda = \frac{L}{R}, \qquad \tau = \frac{D}{2R}, \qquad \xi = \frac{\sigma}{\sigma_{Max}} \tag{1}$$

where L is the maximum ligand extension, D the nearest neighbor NC distance, σ the grafting density and σ_{Max} the maximum possible grafting density. If the NCs are described as hard spheres[23], the nearest neighbor separation is the same as the hard sphere diameters, which is given by the OPM formula[36].

$$\tau = (1 + 3\lambda\xi)^{1/3} \ . \tag{2}$$

The hard sphere description may break down by "vortices", structures consisting of ligands splayed radially outward from the surface they are grafted on[17,18], see Fig. 14 and Fig. 10, whenever the NC coordination is low (≤ 6).

A. Adsorption Energies

The adsorption free energies of an isolated NC to a substrate are quite large, between $50 - 200\ k_BT_m$, or around $1 - 4$ eV. Although the mechanism of NC bonding, attractive Van der Waals forces competing against the reduction in chain entropy, is the same mechanism

in NC adsorption to a substrate, adsorption to the substrate is much stronger, between 10-90 % lower, than for bonding between two NCs because the solid substrate presents a much larger surface cross section for the ligands to adsorb. This is shown by comparison of half the bonding of a symmetric, free floating pair to the single NC adsorption to a substrate, see Table I.

Adsorption is quite sensitive to the NC orientation and is favored along the [111] direction, see Fig. 2, ranging from $11-20\ k_BT_m$, or about $0.15-0.3$ eV, see Table I. These differences are significant and establish that isolated and *equilibrated* NCs orient within the substrate.

As shown in Fig. 12, adsorption energies increase linearly with ligand length and are also dependent on NC core size. This is consistent with adsorption energies being proportional to the vortex, as ligand length and number of grafted ligands dictate the size of the vortex. It is important to note that there are very slight differences in grafting densities among different facets of the NC core, as indicated by slightly varying adsorption energies depending on the NC orientation. Additional analysis of the adsorption energies is given in the supplemental information where the adsorption energy is fitted to the number of adsorbed ligand monomers and other variables specific to the NC.

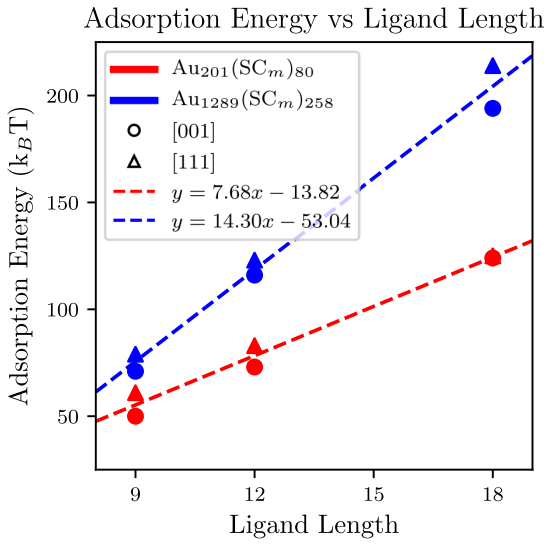

FIG. 12: Plot of adsorption energies as a function of the ligand chain length. Ligand length is given as number of carbons in the ligand chain and adsorption energy is given in k_BT with $T = T_M = 387$ K.

B. NC Nearest Neighbor Separations and Bonding

The histogram of equilibrium nearest neighbor distances is given in Fig. 7. It is apparent that distances are monotonic with coordination. In Fig. 13, we plot the equilibrium distances in a $\tau - \lambda$ plot, see Eq. 1 for notation, together with the OPM result Eq. 2.

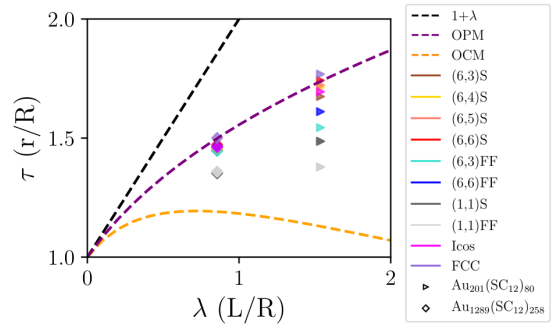

FIG. 13: Plot of τ as a function of λ, see Eq. 1 for notation, for all systems supported by a solid substrate (S). We also include the "Free Floating" (FF) systems considered in previous simulations[19,21,22]. The OPM model is described by Eq. 2, while the OCM is the theoretical lowest possible distance[41]

.

It is apparent from Fig. 13 that the effect of the substrate in the nearest neighbor distance is qualitatively small. This is made more explicit in both Fig. 9 and Fig. 6 where the nearest neighbor separation is higher by about 10% from the free floating case. This is a consequence of the NC-substrate vortex that coalesces with the NC-NC vortex, see Fig. 10 and the discussion in the text.

The bonding of NCs is *weaker* when supported by a substrate as compared to free floating cases, see Fig. 9. However, assembly at the substrate is still favorable, as it also includes the contribution from the free energy of adsorption.

C. Ligand Vortices

In Fig. 14, we provide an average configuration of a single NC adsorbed at the solid substrate. While the ligands are pointing, on average, radially from the core center if not interacting with the substrate, they are splayed when on the surface, i.e., they form a vortex. This nicely illustrates the point made before that the solid substrate behaves as a "giant" NC without functionalized ligands.

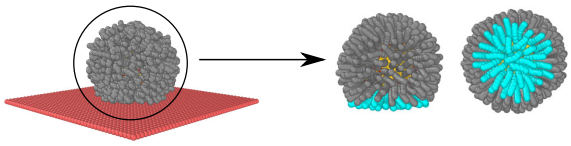

FIG. 14: Example of NC-Substrate vortex formed at PMF minimum for $Au_{1289}(SC_{12})_{258}$ [111]. Ligand chains colored cyan form a vortex.

The ligand conformations in the free floating case and the solid substrate supported case are shown in Fig. 10. The obvious difference is that in the former case, there are two vortices per NC, while only one for the latter. The mismatch between the two vortices within the NC in the solid substrate supported case amounts to a repulsive vortex interaction that leads to an increased nearest neighbor as compared to the free floating case, see $Au_{201}(SC_{12})_{80}$ in Fig. 6. However, if the NC core size is large relative to the ligand length, the repulsive vortex interaction is minimized as shown by the $Au_{1289}(SC_{12})_{258}$ NC in Fig. 6. Increasing the size of the NC core relative to the ligand length effectively separates the vortices on the NC preventing them from interacting due to their greater separation on the core, see Fig. 11.

IV. CONCLUSIONS

We have presented a detailed study on the adsorption and bonding of alkylthiolated NCs in the presence of a solid substrate and have shown that, in comparison to the free floating case, the nearest neighbor distances are larger, which results in weaker NC bonding. Yet, because of the favorable adsorption free energies, assembly on the substrate is overall favored over the free floating case.

The simulations support the Orbifold Topological Model[17,18], with the presence of vortices that determine nearest neighbor distances, see Fig. 14 and Fig. 10. The predictions are in excellent agreement with the experimental results by Boles and Talapin[16], see Fig. 13 and Fig. 1.

Our simulations have explicitly modeled gold NCs cores as truncated octahedra, see Fig. 2, and investigated how the adsorption free energy depends on the core orientation. As shown in Table I, adsorption along the [111] planes is favored by more than a few k_BT. This clearly suggests that, initially, nucleation of a superlattice will proceed by a layer of oriented NCs that should become metastable as it grows towards its bulk structure, where NCs are isotropic, i.e., not oriented. A substrate induced FCC transforming towards a BCC superlattice (Bain Transition), has been observed experimentally[26,27]. A quantitative comparison with our results is not entirely possible, as these experiments were done with PbS or PbSe NCs, which have a different structure and are less stable[42] compared to the alkylthiolated Au cores studied here. Explicit simulations with these NCs will surely provide detailed quantitative comparisons but are unlikely to modify the qualitative picture presented. Thus, we conclude that Bain transitions are a direct manifestation of the ability of the substrate to orient NCs.

We should also mention the experiments in Ref.[43], where NCs were assembled at the air-diethylene glycol and then transferred onto a Carbon substrate. The main difference, however, is that the adsorption at the liquid-vapor interface is likely not very sensitive to the core anisotropy, and therefore, the observed binary phases are the result of NC-NC interactions rather than from the NC-substrate interaction. Further work will be needed to establish this point.

Another important issue is related to the dynamics. In previous works[44,45], we have established that the relaxation times increase with the number of NCs breaking the Maxwell theory of evaporation[46]. The relaxation time scales grow like $N^{2/3}$, where N is the number of NCs assembled, and therefore, are beyond the possibility of a realistic simulation. This is the subject for future work.

SUPPLEMENTARY MATERIAL

Supporting information contains one file with:

- Force Field Parameters.
- Additional figures on NC adsorption.
- Further details about Adsorption energies.

ACKNOWLEDGEMENTS

AT acknowledges many discussions and clarification of their work with I. Coropceanu and D. Talapin. Interest and discussions are also acknowledged from S. Mallapragada and D. Vaknin. The software HOODLT is funded by NSF, DMR-CMMT 1606336 "CDS&E: Design Principles for Ordering Nanoparticles into Super-crystals". AT was supported by DOE through the Ames Laboratory is operated for the U.S. DOE by Iowa State University under Contract DE-AC02-07CH11358. MP was supported by an internship through the DOE SULI program. This work used the Extreme Science and Engineering Discovery Environment (XSEDE), which is supported by National Science Foundation grant number ACI-1548562. Our project within XSEDE is supported by grant TG-MCB140071.

DATA AVAILABILITY

The data that supports the findings of this study are available within the article and the supplementary information.

REFERENCES

[1] S. C. Glotzer and M. J. Solomon, "Anisotropy of building blocks and their assembly into complex structures," Nature Materials **6**, 557–562 (2007).

[2] M. A. Boles, M. Engel, and D. V. Talapin, "Self-Assembly of Colloidal Nanocrystals: From Intricate Structures to Functional Materials," Chemical Reviews **116**, 11220–11289 (2016).

[3]R. L. Whetten, J. T. Khoury, M. M. Alvarez, S. Murthy, I. Vezmar, Z. L. Wang, P. W. Stephens, C. L. Cleveland, W. D. Luedtke, and U. Landman, "Nanocrystal gold molecules," Adv. Mater. **8**, 428–433 (1996).

[4]E. V. Shevchenko, D. V. Talapin, S. O'Brien, and C. B. Murray, "Polymorphism in AB13 Nanoparticle Superlattices: An Example of Semiconductor-Metal Metamaterials," Journal of the American Chemical Society **127**, 8741–8747 (2005).

[5]E. V. Shevchenko, D. V. Talapin, N. A. Kotov, S. O'Brien, and C. B. Murray, "Structural diversity in binary nanoparticle superlattices," Nature **439**, 55–59 (2006).

[6]X. Ye, C. Zhu, P. Ercius, S. N. Raja, B. He, M. R. Jones, M. R. Hauwiller, Y. Liu, T. Xu, and A. P. Alivisatos, "Structural diversity in binary superlattices self-assembled from polymer-grafted nanocrystals," Nature Communications **6**, 10052 (2015).

[7]C. Stowell and B. A. Korgel, "Self-Assembled Honeycomb Networks of Gold Nanocrystals," Nano Letters **1**, 595–600 (2001).

[8]P. Moriarty, M. D. Taylor, and M. Brust, "Nanostructured Cellular Networks," Physical Review Letters **89**, 248303 (2002).

[9]T. P. Bigioni, X. M. Lin, T. T. Nguyen, E. I. Corwin, T. A. Witten, and H. M. Jaeger, "Kinetically driven self assembly of highly ordered nanoparticle monolayers," Nature Materials **5**, 265–270 (2006).

[10]M. N. Martin, J. I. Basham, P. Chando, and S. K. Eah, "Charged gold nanoparticles in non-polar solvents: 10-min synthesis and 2D self-assembly," Langmuir **26**, 7410–7417 (2010).

[11]T. Wen and S. A. Majetich, "Ultra-large-area self-assembled monolayers of nanoparticles," ACS Nano **5**, 8868–8876 (2011).

[12]Q. Guo, M. Xu, Y. Yuan, R. Gu, and J. Yao, "Self-assembled large-scale monolayer of Au nanoparticles at the air/water interface used as a SERS substrate," Langmuir **32**, 4530–4537 (2016).

[13]K. D. Comeau and M. V. Meli, "Effect of alkanethiol chain length on gold nanoparticle monolayers at the air-water interface," Langmuir **28**, 377–381 (2012).

[14]J. Chang, J. Lee, A. Georgescu, D. Huh, and T. Kang, "Generalized On-Demand Production of Nanoparticle Monolayers on Arbitrary Solid Surfaces via Capillarity-Mediated Inverse Transfer," Nano Letters **19**, 2074–2083 (2019).

[15]B. A. Grzybowski, K. Fitzner, J. Paczesny, and S. Granick, "From dynamic self-assembly to networked chemical systems," (2017).

[16]M. A. Boles and D. V. Talapin, "Many-Body Effects in Nanocrystal Superlattices: Departure from Sphere Packing Explains Stability of Binary Phases," Journal of the American Chemical Society **137**, 4494–4502 (2015).

[17]A. Travesset, "Topological structure prediction in binary nanoparticle superlattices," Soft Matter **13**, 147–157 (2017).

[18]A. Travesset, "Soft Skyrmions, Spontaneous Valence and Selection Rules in Nanoparticle Superlattices," ACS Nano **11**, 5375–5382 (2017).

[19]C. Waltmann, N. Horst, and A. Travesset, "Capping Ligand Vortices as "atomic Orbitals" in Nanocrystal Self-Assembly," ACS Nano **11**, 11273–11282 (2017).

[20]C. Waltmann, N. Horst, and A. Travesset, "Potential of mean force for two nanocrystals: Core geometry and size, hydrocarbon unsaturation, and universality with respect to the force field," Journal of Chemical Physics **149**, 034109 (2018).

[21]T. Waltmann, C. Waltmann, N. Horst, and A. Travesset, "Many Body Effects and Icosahedral Order in Superlattice Self-Assembly," Journal of the American Chemical Society **140**, 8236–8245 (2018).

[22]X. Zha and A. Travesset, "Stability and Free Energy of Nanocrystal Chains and Superlattices," Journal of Physical Chemistry C **122**, 23153–23164 (2018).

[23]X. Zha and A. Travesset, "The Hard Sphere Diameter of Nanocrystals (Nanoparticles)," Journal of Chemical Physics **152**, 094502 (2020).

[24]J. Xia, N. Horst, H. Guo, and A. Travesset, "Superlattices of nanocrystals with polystyrene ligands: From the colloidal to polymer limit," Macromolecules **52**, 39 (2019).

[25]I. Coropceanu, M. A. Boles, and D. V. Talapin, "Systematic Mapping of Binary Nanocrystal Superlattices: The Role of Topology in Phase Selection," Journal of the American Chemical Society **141**, 5728–5740 (2019).

[26]K. Bian, J. J. Choi, A. Kaushik, P. Clancy, D.-M. M. Smilgies, and T. Hanrath, "Shape-Anisotropy Driven Symmetry Transformations in Nanocrystal Superlattice Polymorphs," ACS Nano **5**, 2815–2823 (2011).

[27]M. C. Weidman, D.-M. M. Smilgies, and W. A. Tisdale, "Kinetics of the self-assembly of nanocrystal superlattices measured by real-time in situ X-ray scattering," Nature Materials **15**, 775–781 (2016).

[28]W. Sun, "Interaction forces between a spherical nanoparticle and a flat surface," Physical Chemistry Chemical Physics **16**, 5846–5854 (2014).

[29]K. M. Salerno, D. S. Bolintineanu, J. M. D. Lane, and G. S. Grest, "Ligand structure and mechanical properties of single-nanoparticle-thick membranes," Physical Review E **91**, 062403 (2015).

[30]Z. Cao, M. J. Stevens, J. M. Y. Carrillo, and A. V. Dobrynin, "Adhesion and wetting of soft nanoparticles on textured surfaces: Transition between Wenzel and Cassie-Baxter states," Langmuir **31**, 1693–1703 (2015).

[31]M. Feldmann, D. Dietzel, A. Tekiel, J. Topple, P. Grütter, and A. Schirmeisen, "Universal Aging Mechanism for Static and Sliding Friction of Metallic Nanoparticles," Physical Review Letters **117**, 025502 (2016).

[32]G. D. Förster, F. Rabilloud, and F. Calvo, "Adsorption of metal nanoparticles on carbon substrates and epitaxial graphene: Assessing models for dispersion forces," Physical Review B - Condensed Matter and Materials Physics **91**, 245433 (2015).

[33]S. Nayak, N. Horst, H. Zhang, W. Wang, S. Mallapragada, A. Travesset, and D. Vaknin, "Ordered Networks of Gold Nanoparticles Crosslinked by Dithiol-Oligomers," Particle and Particle Systems Characterization **35**, 1800097 (2018).

[34]S. Nayak, N. Horst, H. Zhang, W. Wang, S. Mallapragada, A. Travesset, and D. Vaknin, "Interpolymer Complexation as a Strategy for Nanoparticle Assembly and Crystallization," Journal of Physical Chemistry C **123**, 836–840 (2019).

[35]H. J. Kim, W. Wang, A. Travesset, S. K. Mallapragada, and D. Vaknin, "Temperature-Induced Tunable Assembly of Columnar Phases of Nanorods," ACS Nano **14**, 6007–6012 (2020).

[36]U. Landman and W. D. Luedtke, "Small is different: energetic, structural, thermal, and mechanical properties of passivated nanocluster assemblies," Faraday Discussions **125**, 1–22 (2004).

[37]J. A. Anderson, C. D. Lorenz, and A. Travesset, "General purpose molecular dynamics simulations fully implemented on graphics processing units," Journal of Computational Physics **227**, 5342–5359 (2008).

[38]T. D. Nguyen, C. L. Phillips, J. A. Anderson, and S. C. Glotzer, "Rigid body constraints realized in massively-parallel molecular dynamics on graphics processing units," Computer Physics Communications **182**, 2307–2313 (2011).

[39]A. Travesset, "Phase diagram of power law and Lennard-Jones systems: Crystal phases," Journal of Chemical Physics **141**, 164501 (2014).

[40]S. Kumar, J. M. Rosenberg, D. Bouzida, R. H. Swendsen, and P. A. Kollman, "The weighted histogram analysis method for free-energy calculations on biomolecules. I. The method," Journal of Computational Chemistry **13**, 1011–1021 (1992).

[41]P. Schapotschnikow and T. J. H. Vlugt, "Understanding interactions between capped nanocrystals: Three-body and chain packing effects," The Journal of Chemical Physics **131**, 124705 (2009).

[42]M. A. Boles and D. V. Talapin, "Binary Assembly of PbS and Au Nanocrystals: Patchy PbS Surface Ligand Coverage Stabilizes the CuAu Superlattice," ACS Nano **13**, 5375–5384 (2019).

[43]T. Udayabhaskararao, T. Altantzis, L. Houben, M. Coronado-Puchau, J. Langer, R. Popovitz-Biro, L. M. Liz-Marzán, L. Vukovic, P. Král, S. Bals, and R. Klajn, "Tunable porous nanoallotropes prepared by post-assembly etching of binary

nanoparticle superlattices," Science **358**, 514–518 (2017).
[44]T. Waltmannn and A. Travesset, "Assembly by solvent evaporation: equilibrium structures and relaxation times," Nanoscale **11**, 18702–18714 (2019).
[45]E. Macias, T. Waltmann, and A. Travesset, "Assembly of nanocrystal clusters by solvent evaporation: Icosahedral order and the breakdown of the Maxwell regime," Soft Matter **16**, 7350–7358 (2020).
[46]N. Fuchs, *Evaporation and Droplet Growth In Gaseous Media*, i ed. (Pergamon Press, 1959) pp. 1–72.